LIMITS ON THE ACCURACY OF DRIFT CHAMBERS AND CALIBRATION BEAMS

Bernard Sadoulet
CERN, Geneva, Switzerland

1. Introduction

A glance at the letters of intent for experiments at LEP which have been submitted to CERN on 31 January 1982 show that drift chambers of one type or another are still very popular and are considered as being the main candidate for detecting charged particles even eight years from now.

The understanding of intrinsic limits on the spatial accuracy of drift chambers, and the development of new methods for calibrating them, are therefore still relevant. The present talk attempts to review the state of the art.

In order to see what are the main questions to be asked, I have summarized in Table 1 the main characteristics of the drift-chamber detectors proposed for LEP. These detectors fall into two classes:

i) Extremely accurate detectors for vertex reconstruction around the interaction region. Precision as high as 30 μm is looked for and two-particle resolution of 200 μm is claimed. In this field, competition from multi-electron silicon detectors[1], which could reach 10 μm accuracy and 150 μm resolution, is severe.

ii) Very large detectors of the projection-chamber or imaging-chamber type, where the moderate accuracy of individual measurement ($\sigma_w \simeq 200$ μm) is compensated by the relatively large number of points on each track. The accuracy of the momentum measurement is no longer limited by the drift-time precision but by the control of systematics at the level of 30 to 50 μm on the sagitta.

Hence the two questions studied in this talk:

i) What are the fundamental limits on the accuracy and the two-particle resolution in a gaseous drift chamber (Section 2)? How can performances be improved, by the proper choice of gas and running

Table 1

A glance at LEP letters of intent

Collab.	Detector	Method	Dimensions	Accuracy	Two-particle resolution
Bari, etc.*)	Minivertex	Silicon			
	Main	TPC 1 atm, 1.5 T	$0.2 < R < 1.8$ m $\ell = 4.4$ m $d = 2.2$ m	$\sigma_M \leq 200$ μm (21 space pts)	$R\phi = 1.2$-2.4 cm $z = 1.5$ cm
		— or —			
		Axial wires 1 atm, 1.5 T	$0.2 < R < 1.8$ cm $\ell = 4.4$ m $d = 8$ cm	$\sigma_M \leq 250$ μm (192 wires)	$R\phi = 0.75$ cm
OPAL	Main	JADE-like 4 atm, 1 T	$R < 1.6$ m	$\sigma_M = 100$ μm (160 wires)	$R\phi = 0.2$ cm
Lund, etc.**)	Minivertex	Time expansion + side wire pick ups or silicon	$0.065 < R < 0.125$ $\ell = 0.45$ m $d = 3$ mm $0.15 < R < 0.5$ $d = 6$ mm	$\sigma_M = 30$ μm $\sigma_M = 100$ μm	$R\phi = 0.02$ cm
	Main (μ)	Planar imaging chamber	$R < 3.8$ m $\ell = 6$ m	$\sigma_M \sim 250$ μm $\Rightarrow \sigma_s \lesssim 30$ μm	
Electra	Minivertex	Axial drift wires	$R < 0.38$ m $\ell = 2$ m	$\sigma_M = 50$ μm (24 wires)	
	Main	Conventional drift chambers with stereo, 1 T	$R < 1.2$ m $\ell = 4.5$ m $d = 1$ cm	$\sigma_M = 150$ μm (40 wires)	
DELPHI	Minivertex	Drift chambers with cathode strips	$R < 0.3$ m	$\sigma_M = 100$ μm	$R\phi = 1$ mm
	Main	TPC 1 atm, 1.2 T	$0.3 < R < 1.26$ m	$\sigma_M = 250$ μm	
LOGIC	Main	JADE-like	$0.1 < R < 0.7$ m $\ell = 2$ m	(64 wires)	

*) Bari-CERN-Demokritos Athens-Dortmund-Ecole Polytechnique-Palaiseau-Edinburgh-Glasgow-Heidelberg-Lancaster-MPI Munich-Orsay-Pisa-Rutherford-Saclay-Sheffield-Trieste-Turin-Westfield College London-Wisconsin Collaboration.

**) Lund-Siegen-Max Planck Institute-NIKHEF-ETH-Geneva-Lausanne-LAPP-Frascati-Florence-Madrid-Beijing-Hofei-Hawaii-CalTech-Oklahoma-Ohio State-Carnegie Mellon-Princeton-Yale-Harvard-MIT Collaboration.

conditions, or by better detection methods (Section 3)?

ii) What, in practice, are the limits encountered in large detectors? Is it possible to limit effects of systematics by proper design of the detector (Section 4)? Can X-ray and UV calibration beams be used (Section 5)? Since most of the other talks presented at this conference will deal with specific practical aspects, I will emphasize mainly the fundamental aspects and the understanding of the basic mechanisms.

* * *

It is clear that, in this review, most of the quoted results and explanations are not mine, and I profited very much from discussions with many colleagues. I would like to thank especially G. Charpak, B.A. Dolgoshein, C. Rubbia, H.A. Walenta and T. Ypsilantis, from whom I have borrowed many ideas put forward in this talk.

2. Fundamental Processes in Drift Chambers

Let us recall the basic processes at work in a drift chamber[2]. Electrons are produced along charged particle trajectories (Fig. 1). They then drift in an electric field towards a detecting cell where they are observed. More and more often the detection is bidimensional, which together with the drift-time measurement allows the reconstruction in space of the extraction point of the original electrons. Let us review each of the successive phases in turn.

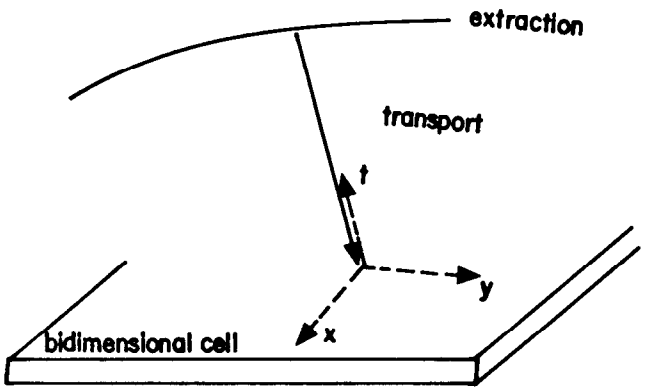

Fig. 1. A drift chamber of the projection or imaging type.

2.1 Extraction and Thermalization of the Electrons

The extraction of primary electrons by a charged particle of velocity βc is now well understood quantitatively[3] as the result of an exchange of a virtual photon which ionizes the gas molecule. The differential cross-section can be written as

$$\frac{d\sigma}{dE} = \int_{E/\beta c}^{\infty} dp\, f(E,p) \left(\frac{1}{E^2 - p^2c^2} \right)^2 \sigma_\gamma(E,p) \ , \qquad (1)$$

where E and p are the energy and momentum transferred to the extracted electron; $f(E,p)$ describes the particle-photon vertex; $\sigma_\gamma(E,p)$ is the off-shell photoionization of the gas molecule which can be approximated[3] by the on-shell photoionization cross-section at low energy (shown in Fig. 2a for argon) and the Rutherford cross-section for large E where electrons are quasi-free. The result for argon is given in Fig. 2b. The various M, L, and K shell peaks appear very clearly.

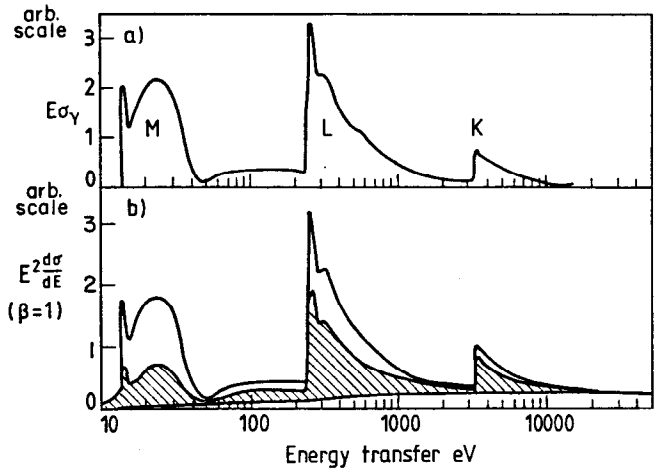

Fig. 2. a) Photoionization cross-section for argon. b) Differential cross-section for the extraction of electrons by a relativistic charge-1 particle (Ref. 3).

The energy is deposited in a discrete way at the macroscopic level. For instance, in argon there are about 30 electrons per cm extracted from the M shell with a typical energy of 30 eV, about 1.5 cm from the L shell with 400 eV, 0.03 cm from the K shell with a typical energy of 4 keV, and 0.03 cm for δ-rays above 4 keV.

Then these electrons slow down by inelastic collisions, through which they extract both photons and electrons until they reach an equilibrium temperature with the electric field and begin to drift. The total number of electrons at the end of the thermalization process is on an average proportional to the deposited energy, with a fairly small fluctuation

$$n_T = \frac{\Delta E}{E_i} \ . \qquad (2)$$

For argon n_T is of the order of 100 electrons/cm.

What matters for drift-chamber application is the distance reached transversally by the slowing down electrons. This practical range of their trajectories, which are convoluted by multiple scattering, is not very well studied either theoretically or experimentally. The best data available to my knowledge are the measurements of absorption lengths of low-energy electrons in gases by Lenard[4], quoted by Farr et al.[5]. According to this result, in argon at atmospheric pressure one gets a mean absorption length smaller than 0.5 μm for an M-shell electron, about 1 μm for an L shell electron of 400 eV, and 15 μm for a K-shell or δ-ray electron of 4 keV. Extrapolations from results in light materials[6] give absorption lengths which are 10 to 20 times longer. However, this shows that for the more numerous electrons (M and L shell electrons) the practical range is very small and the half radius of the electron blob is usually of the order of 10 to 20 μm at most at nominal pressure and temperature.

2.2 The Drift Region

In the drift region, electrons make a random walk between the molecules. Let us first discuss their behaviour in the absence of magnetic field. They are accelerated between successive collisions in which they lose part of their energy and their initial direction. They can be described by the distribution $F(v, \cos\theta)$ of their random velocity v and their angle θ with the electric field. In the absence of magnetic field their drift velocity w_L (much smaller than their random velocity) is then

$$w_L = \int v \cos\theta \, F(v, \cos\theta) \, dv \, d\cos\theta \qquad (3)$$

and their mobility is $\mu = w_L/E$.

Their fluctuation around the average position $z = z_0 + w_L t$ (z along the electric field) is controlled by two diffusion coefficients D_T and D_L

$$\frac{d\langle z^2\rangle}{dt} = 2D_L$$
$$\frac{d\langle \delta x^2\rangle}{dt} = \frac{d\langle \delta y^2\rangle}{dt} = 2D_T \, . \qquad (4)$$

D_T is given by

$$D_T = \int \frac{\ell v}{3} F(v, \cos\theta) \, ,$$

where ℓ is the mean free path. One can also introduce the characteristic energy

$$\varepsilon_K = eD_T/\mu \, , \qquad (5)$$

which is related to the average energy of electrons. It is bounded from below[1] by kT, which therefore means that the transverse diffusion of an electron cloud after a drift distance z

$$\sigma_x = \sigma_y = \sqrt{\frac{2D_T z}{w}} = \sqrt{\frac{2\varepsilon_k z}{eE}} \qquad (6)$$

is bounded by

$$\sigma_x = \sigma_y = \sqrt{\frac{2kTz}{eE}} \, . \qquad (7)$$

Figure 3 gives experimental measures of D_T and some theoretical estimates[2]. The longitudinal diffusion coefficient is given by a more complicated expression[7]. It is different from the transverse coefficient because electrons which have by fluctuation gone faster than the average drift velocity are more energetic since the work of the electric field has been bigger. They are therefore less affected by this field, and their drift velocity is smaller than the average one. Therefore one expects that

$$D_L \leq D_T \, .$$

This statement is true provided the electron momentum transfer cross-section does not decrease too fast and it can be shown on semiquantitative models[7] that the faster the cross-section increases, the smaller is the ratio D_L/D_T.

The gain can be very significant, as shown in Fig. 4 for argon. At low energy $eD_L/\mu \approx eD_T/\mu \approx kT$ when the electrons are in thermal equilibrium with the gas. Then the longitudinal diffusion increases faster than the transverse diffusion because the cross-section decreases. At $E/N \approx 4 \times 10^{-19}$ V/cm^2 the mean electron

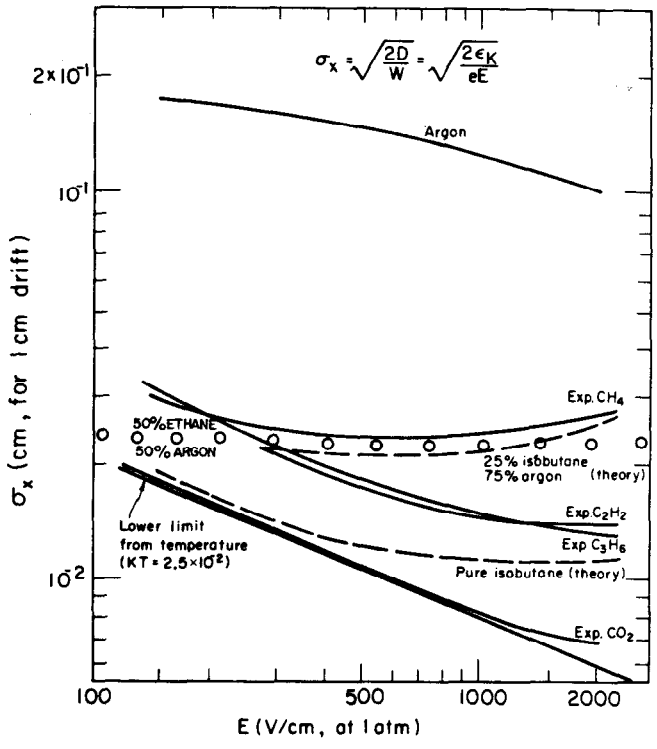

Fig. 3. Transverse diffusion σ_x after 1 cm of drift for various gases.

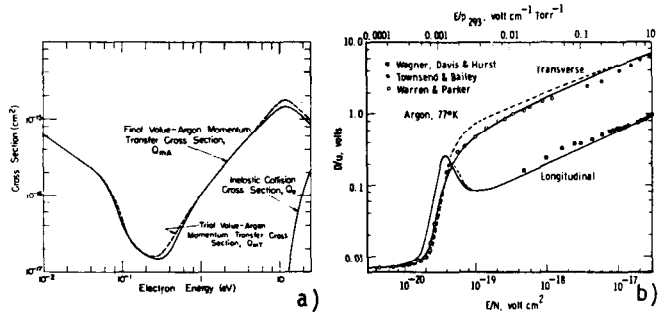

Fig. 4. a) Momentum transfer cross-section for argon (e.g. Ref. 2). b) Transverse and longitudinal diffusion in argon (Ref. 7).

energy reaches 0.2 eV where the cross-section displays a minimum, and when the cross-section begins to increase D_L drops quite significantly to a value seven times smaller than D_T.

This behaviour of the cross-section is also responsible[2] for the saturation of the drift velocity in most argon hydrocarbon mixtures. Theoretically one expects therefore two situations

i) In "cool" gases (e.g. CO_2) the electrons have temperatures of the order of kT; D_L and D_T are comparable and low but, however, the drift velocity is proportional to the field.

ii) In mixtures with saturated drift velocity, the electrons have higher temperatures but D_L can be significantly smaller than D_T.

In addition to the classical measurements of Wagner, Davis and Hurst[8], new measurements have been made recently by various high-energy physics groups[9-12].

As an example, Fig. 5 gives the longitudinal diffusion σ_z after 1 cm of drift for various gases.

Values of typically $\sigma_z = 250\ \mu m/cm^{1/2}$ are obtained for an electric field between 500 V/cm and 1 kV/cm at normal pressure with argon-CO_2, argon-C_2H_6, and argon-C_4H_{10}. The value for argon-CH_4 is higher around $400\ \mu m/cm^{1/2}$. Pure organic vapour or CO_2 have significantly smaller diffusion.

When there is a magnetic field, electrons are not only accelerated by the electric field but are also deflected by the magnetic field. If the magnetic field is perpendicular to the electric field, electrons will drift at an angle α_D often written as

$$\text{tg}\ \alpha_D = w_M \frac{B}{E}\ , \qquad (8)$$

where w_M is the so-called magnetic drift velocity which is somewhat larger than w_L in standard mixtures. The drift velocity w_L along the electric field is affected also, but usually the drift velocity along the electron trajectories is rather constant.

When the magnetic field is parallel to the electric field the transverse diffusion is decreased because the electrons have a tendency to curl in between collisions. However, the reduction factor which is approximately

$$1 + \frac{3}{2}\frac{B^2}{E^2} w_L^2$$

is usually quite close to one.

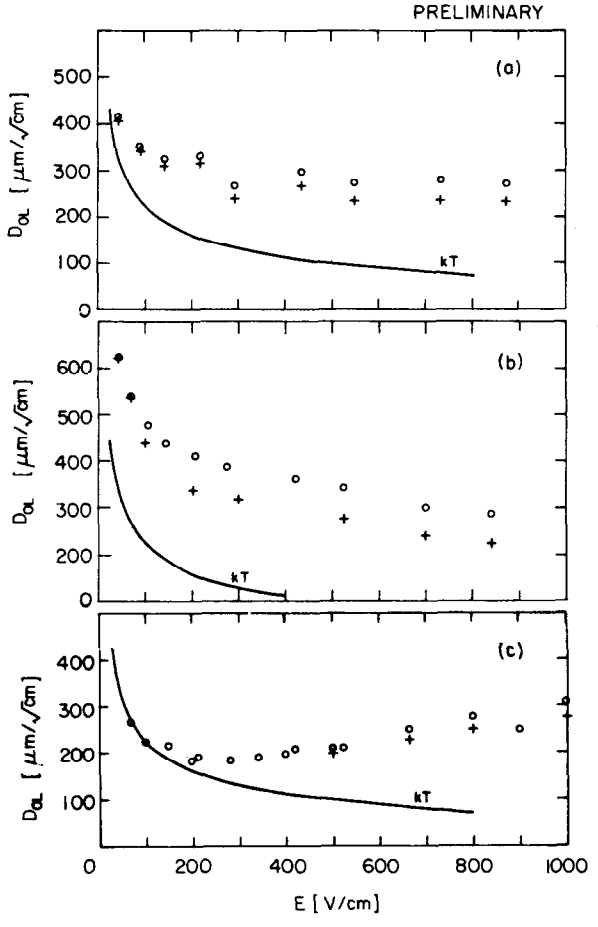

Fig. 5. Longitudinal diffusion σ_z after 1 cm of drift for various gases (Ref. 12): a) Argon C_2H_6 (50-50); b) argon CH_4 (80-20); c) argon CO_2 (80-20). Circles are raw measurements. Crosses are corrections for dispersion due to the differences of electron trajectories.

2.3 The Detecting Cell

After the drift region, the electrons arrive at the detecting cell. The usual method is to have them multiply in the high-field region surrounding a thin "sense" wire. This method has two consequences.

i) Because the field is cylindrical around the sense wire, some electrons exiting from the drift region far from the sense wire will have to travel longer. Moreover they encounter regions of lower electric field. As a consequence the loci of equal time of arrival on the sense wire are not planes but rather cylinders. Therefore, even for tracks perpendicular to the average drift direction, extracted electrons do not arrive on the wire at the same time. Figure 6 shows as an example the case of the UA1 detector in a field of 7 kG.

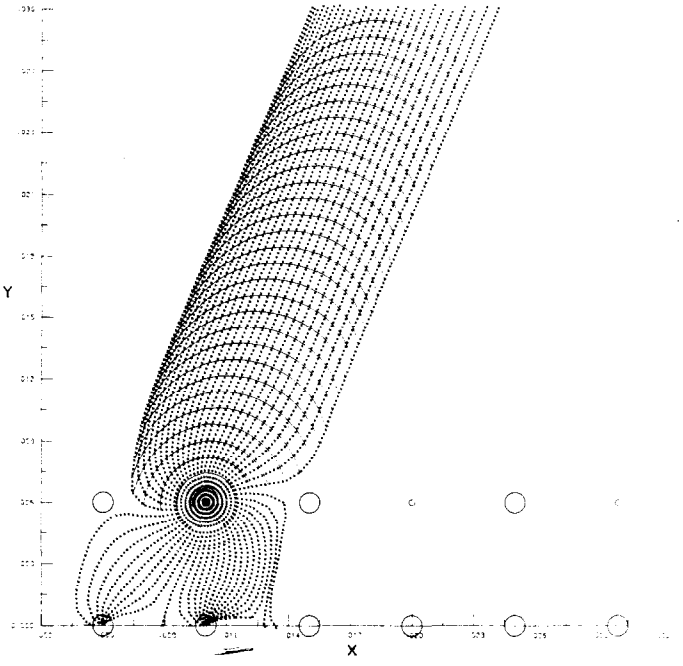

Fig. 6. Electron trajectories and loci of equal drift time from the sense wire in the central detector of UA1 (electric field = 1.5 kV/cm, magnetic field = 7 kG).

ii) The electric pulse which is recorded on the sense wire or on cathode pads is mainly due to the movement of the ions in the 1/r electric field around the wire. This gives to the electric current pulse a long tail in 1/t which without proper shaping limits two-particle resolution. Note that this tail is absent in the detection by scintillation light[13].

Parallel-plate chambers[14] where the multiplication occurs in a planar electric field do not have these problems. However, for tracks at an angle with the electric field, it is unavoidable that the electron clusters arrive in the detecting cell at different times.

In order to record the original position of the primary electron in space, two methods are used:

i) Drift-time measurement with usually a constant threshold discriminator. The measurement is therefore sensitive to the longitudinal diffusion σ_z.

However, the measurement error σ_w is smaller. In a system that is sensitive to the first electron

$$\sigma_w = \frac{1.28\ \sigma_z}{\sqrt{2 \log n}} , \qquad (9)$$

where n is the number of electrons in the cloud. However, if the centre of gravity was detected

$$\sigma_w = \frac{\sigma_z}{\sqrt{n}} . \qquad (10)$$

In practice, σ_w is smaller than σ_z by a factor of 2 to 3 yielding

$$\sigma_w \approx 80\text{-}125\ \mu m/cm^{1/2}$$

for usual argon-organic vapour mixtures and fields.

ii) Centre of gravity with cathode-pad amplitude read-out. The measurement is sensitive to the transverse diffusion σ_x but, in the approximation where electrons are assumed to arrive at the same time, the centre of gravity is measured and

$$\sigma_w = \frac{\sigma_x}{\sqrt{n}} .$$

In principle, better accuracies can be achieved with this method (if the preamplifier noise is small enough). However, if the track is at an angle to the sense wire, fluctuations in the primary ionization leads to substantial degradation of accuracy at low pressure[15].

3. Ways to Improve the Accuracy and to Obtain Better Two-Particle Resolutions

The understanding of the various factors controlling accuracy and two-particle resolution is therefore rather good. There is not much which can be gained in the extraction mechanism of electrons. Most of the electrons have ranges smaller than 10 or 20 μm under normal conditions and the few per cent of long-range δ-rays can be rejected either by pulse height or by deviation from the fitted track.

3.1 Decreasing Diffusion

Quite significant gains can be achieved in principle on the transverse or longitudinal diffusion.

i) A first obvious choice is to reject "hot" gases such as A_2-CH_4 mixtures where the diffusion is quite large.

It is clear that argon-organic vapour gives higher diffusion and should be abandoned in high-accuracy applications in favour of pure gases such as CO_2 [8], C_2H_4 [8], and C_4H_{10} [2].

In CO_2 (Figs. 7a, b) electrons are practically thermal, which means that the drift velocity is proportional to the electric field. It is a bad quencher, but adding a few per cent isobutane considerably improves proportional operation[16].

Ethylene is a good candidate: electrons are not thermal and the drift velocity, although not saturated, does not vary too rapidly (Fig. 7d). It has the nice property of having a longitudinal diffusion which is much lower than the transverse diffusion and which is only slightly higher than that of CO_2. In practice, a better quencher, such as methylal[10], has to be added to the gas.

With these two gases, one can reach

$$\sigma_z \approx 80\text{-}100\ \mu m/cm^{1/2} \quad \text{at 1 kV/cm} ,$$

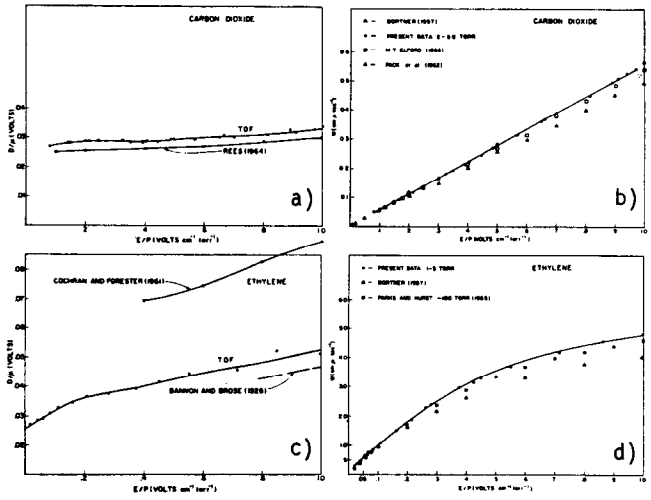

Fig. 7. Drift velocities and diffusion coefficients for CO_2 and C_2H_4. The horizontal axes are E/p (volts/cm torr). The vertical axes for a) and c) are D/μ (volts); the vertical axes for b) and d) are W (cmμ/sec).

which is significantly smaller than the usual values obtained in argon-organic vapour mixtures.

ii) The second parameter that we can use is the pressure P. The ratio eD/μ is a function of E/P only. Therefore increasing P and E proportionally allows one to decrease σ

$$\sigma_z = \sqrt{\frac{eD}{\mu E}} \propto \sqrt{\frac{1}{P}} \quad (E/P = \text{const.}) . \qquad (11)$$

In practice, for non-thermal gases, eD/μ is a weak function of E/P and nearly the full gain is obtained by increasing P only. In addition, the electron statistics are improved[5], and through Eq. (9) the measurement accuracy will be improved even further. Dolgoshein and collaborators[16] have attempted to make full use of this property by going to extreme pressures. By going to 300 atm in an argon (99%) + N_2 (1%) mixture they have reached

$$\sigma_z = 10\text{-}15\ \mu m/cm^{1/2}$$

(measured with scintillation light). Limits are encountered, however, in that direction. Multiple scattering in the wall of the pressure vessel weakens the power of such detectors. Moreover, whether scintillation or electron multiplication is used for detection, only a very small amount of quenching molecules can be added to the noble gas used, and the electron temperature is much higher than in the usual mixture.

It seems more promising to work at lower pressure, where these problems are simplified. This approach was explored rather systematically by Farr et al.[5] and then used by the JADE Collaboration[9] (whose experiment runs at 4 atm with an argon-CH_4-C_4H_{10} mixture, which is unfortunately not very good having $\sigma_z = 400\ \mu m/cm^{1/2}$ at 1 atm). Dolgoshein and collaborators[17] have pushed this line of research quite far. Using CO_2 at 5 atm (with 0.3 atm of C_4H_{10}), they obtain a drift measurement accuracy of

$$\sigma_w = 25\ \mu m$$

over a drift length of 12 mm and a drift voltage of 3.5 kV. Allowing only clusters produced directly in line with the sense wire to reach it and shaping carefully the pulses, the two-particle resolution at 50% efficiency is 70 μm (the drift velocity w_L is approximately

5×10^5 cm/s). Increasing the pressure does not cause any improvement because of the setting up of parasitic phenomena which are not well understood yet (deviation from E/P behaviour, etc.).

We are not very far from multielectrode silicon detectors with a much simpler technology!

3.2 Can One Detect Original Clusters?

Another place for improvement is the detection method. In principle if the original clusters could be located in *space*, the measurement accuracy will finally be

$$\sigma_w = \frac{\sigma_z}{\sqrt{n}}$$

in spite of the difference of trajectories of the electrons. Since the total number of electrons n is fairly large ($\sim$ 100 cm under normal conditions), improvement by a factor as large as 3 or 5 can theoretically be made on the standard method. Moreover, since all the information is used magnificent two-particle resolution and dE/dx accuracy can, in principle, be obtained[18].

What does cluster detection require?

i) A careful shaping of the pulses with proper clipping of the 1/t tail. Full widths at half maximum of 15-20 ns have been achieved[19].

ii) The drift velocity should be low enough so that this width should be smaller than the natural width of the electron swarm that one wants to separate into clusters. In order to find the centre of gravity of the cloud, a width comparable to that of diffusion is presumably sufficient.

In order to decrease the drift velocity, Walenta[18] proposed to reduce the electric field in the gap (time expansion chambers). Another method is to use a slow gas like CO_2. As we have seen, superb two-particle resolution can be achieved that way[16].

iii) Various methods have been proposed in order to get rid of the drift-time difference of clusters originating from different places along the track.

The simplest one is to prevent electrons with long drift paths from reaching the sense wire, either mechanically[16] (Fig. 8a) or electrostatically (Fig. 8b). Of course one loses information.

A more ambitious approach has first been proposed, to my knowledge, by Walenta[20a]: he suggests measuring the angle of impact of the electron cluster on the sense wire, therefore allowing the reconstruction of its trajectory and correction for the longer path in the cylindrical region around the wire. This can be done by analysis of the induced pulses on cathode pads around the wire (Fig. 8c) or on two pick-up wires close to the anode (Fig. 8d). Experimentally for X-rays an angular resolution of $\Delta\alpha = 5°$ FWHM has been achieved by measuring the difference between the two induced pulses. For charged particles such a difference would have to be normalized to the sum of the two pulses.

iv) Although zero crossing methods can be tried[20], the discrete nature of the production of electrons will produce direct and induced pulses of a vast variety of shapes which cannot really be treated by hardware. It is probably more promising to use Flash ADCs to register directly the pulse height in bins comparable to the clipped pulse width.

We may therefore conclude that the technique exists to reconstruct cluster origins with accuracy limited by the longitudinal diffusion. It has to be shown in practice that the expected gain in accuracy can be achieved (in spite of local space-charge problems) and that the additional complexity is worth the effort. Note that this complexity is not much bigger than for cathode pads.

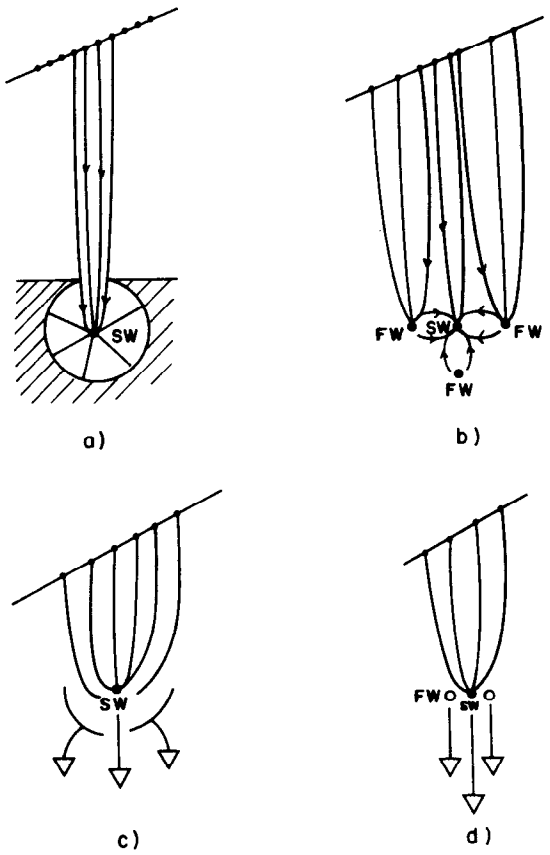

Fig. 8. How to get rid of drift time differences between clusters originating from different places along the track.

4. Systematic Errors in Drift Chambers

We now turn to more practical problems -- encountered especially in large detectors such as JADE, AFS, or UA1 -- which are not limited by the measuring error of each sense wire but by systematics.

4.1 Mechanical Distortion and Stability

It is obvious that the bigger the detector, the more difficult it is to position the wires with sufficient accuracy. Moreover, electrostatic forces and gravity displace the wires by significant amounts in their middle.

In principle, the deviations from a theoretical detector are smooth and can be calibrated away. However, it is difficult to measure these distortions accurately from survey, for instance, and they should be sufficiently stable. Unfortunately, some deformations of large mechanical assemblies are due to temperature gradient, settlement of the supporting structure, etc., and vary with time.

Care has therefore to be exercised in limiting temperature variation of structural elements (good cooling of preamplifiers), in the proper design of the mechanics, and in the method of construction. Dynamic positioning of detector elements has been proposed[20b]. Ultimately, zero-field tracks and calibration beams have to be used (see next section).

4.2 Knowledge and Stability of Drift Velocity and Drift Angle

For detectors with large drift gap the knowledge of drift velocity w_L and drift angle is critical. In order to get 100 μm accuracy over 20 cm, w_L has to be known to 5×10^{-4}.

In order not to be too sensitive to temperature variation, distortion in electric field, and variation with gas mixture, the drift velocity should vary as slowly as possible with these parameters. However, the requirements are often contradictory.

In the case of an electric field perpendicular to the magnetic field, a more serious problem is encountered with the drift angle which varies rapidly with the magnetic field and the electric field [Eq. (8)]. One should therefore minimize its influence by reducing it as much as possible (high field, proper choice of gas) and by arranging the detector so that particle trajectories are perpendicular to drifting electron trajectories. In that case drift-angle errors are zero to second order ("cosine" error). The Bari-CERN-Demokritos Athens-Dortmund-Ecole Polytechnique Palaiseau-Edinburgh-Glasgow-Heidelberg-Lancaster-MPI Munich-Orsay-Pisa-Rutherford-Saclay-Sheffield-Trieste-Turin-Westfield College London-Wisconsin Collaboration has proposed an original arrangement of drift cells (Fig. 9) for LEP which has this property for a solenoidal field.

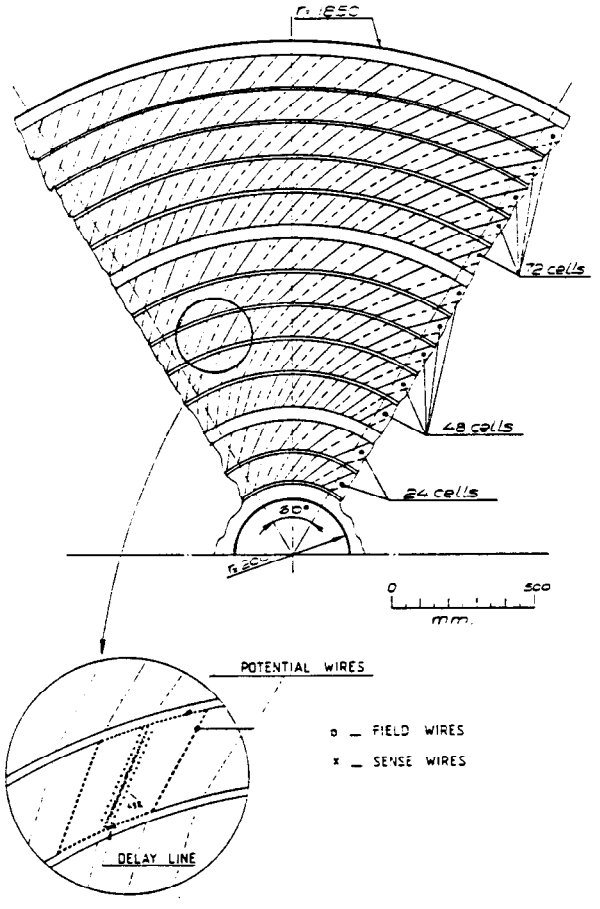

Fig. 9. Proposal for an axial wire drift chamber for LEP by the Bari-CERN-Demokritos Athens-Dortmund-Ecole Polytechnique Palaiseau-Edinburgh-Glasgow-Heidelberg-Lancaster-MPI Munich-Orsay-Pisa-Rutherford-Saclay-Sheffield-Turin-Trieste-Westfield College London-Wisconsin Collaboration (January 1982).

As a general comment, I would like to stress that, instead of trying to measure and monitor all parameters on which the drift velocity and drift angle depend, it is much better to measure them directly in the chamber. This can be done very well in two ways:

i) The chambers can be designed in such a way as to be "autocalibrating". If tracks can cross different drift gaps, which have a constant and known relationship, the requirement that they line up is a powerful constraint on the drift velocity and drift angle. We have found this to be extremely useful in the UA1 detector[21]. Note that this property is absent in normal TPCs or in the JADE-AFS bicycle-wheel structure, but present in designs such as the one of Fig. 9.

ii) A second method[22] is to use several laser beams at fixed and known angles with respect to each other. The drift velocity and drift angle have to be such that the angles are reconstructed correctly. This method is independent of angular correction which make more direct methods impracticable.

4.3 Distortion of Electric Field

In projection or imaging chambers, where the drift gaps are fairly large, the electric field can be compared to the optics in a visual detector.

Tilting of the field direction or change in its magnitude (which changes drift velocity and, more seriously, drift angle) can be caused either by wrong design (too rough shaping of the field), mechanical displacement of the shaping electrodes, or charging up of insulating material in the chamber.

To these static effects could be added dynamical effects due to a positive ion-current in the gap. If ions are collected by shaping electrodes their voltage should be maintained by a divider with low enough impedance. And by their mere presence in the gap the ions create a global space charge which distorts the electric field[23] and is one of the most fundamental limits to the projection-chamber idea.

One can show[23] that for a given particle illumination and amplification the distortion goes as the cube of the drift gap. For detectors in a large background environment, gaps cannot be very large. This was, for instance, a reason to limit the gap in the UA1 central detector to 18 cm since, with a uniform background of 10 mrem/h, distortion of 110 μm in the electric field direction (at an amplification of 10^5) is already caused. The avalanche gain is decreased by about 5%. Non-uniform illumination will produce stronger displacement.

Apart from decreasing the gap length, space charge can be controlled by decreasing the amplification and the proportion of ions which come back to the drift gap. This is difficult because they have a tendency (in the absence of magnetic field) to drift back along the same trajectories as the original electrons. Various pulsed shielding techniques, where pick-up on the sensing elements is minimized by proper balancing, have been proposed in order to turn on the amplification only for interesting events. However, they require a triggering device and may be difficult to implement in large systems.

Another method, since the main effect of space charge is through the drift angle, is to design chambers where errors in drift angle introduce only cosine-like errors.

Once all possible precautions have been taken in the design, one has to learn how to live with space charge. It can be noted that the maximum field distortion occurs in the middle of the drift gap (where it is corrected less by charge images). This induces an apparent curvature of the trajectories in a gap. With what we called an "autocalibrating" chamber, where tracks

usually cross several gaps, the tracks will appear as wiggly lines and fits will partially correct the effect.

One can also imagine using a UV laser beam fired regularly or immediately after a potentially interesting event, which would make a "photograph" of the space-charge situation in the detector.

4.4 Presence of Other Particles

For completeness, we should mention a fourth effect which makes life difficult in practical detectors, namely the presence of other particles close by the particle to be measured, or the fact that the particle is at a large angle to the drift direction.

An obvious first effect is the confusion between two particles, which suppresses a certain number of points along the trajectories and therefore degrades the pattern recognition capability and the accuracy. What we have said on the decrease of diffusion and the improvement of the detecting method for better two-particle resolution is relevant here.

However, more subtle effects occur through cross talk. Some cross talk occurs in the chamber through the movement of ions, which produces positive pulses on neighbouring wires. This can be decreased at the few per cent level by interposing field wires. Their decoupling, however, should be good enough to prevent any significant potential surge which by capacitance will induce a signal on the sense wires. Similarly precautions have to be taken on the packaging and decoupling of the electronics in order to prevent parasitic induction.

Another fundamental effect at work is the possibility of local space charge from previous avalanches disturbing the amplification of the successive electrons. This effect is mainly present for tracks at a large angle to the wire planes.

Here again, in order to extract all the information which is contained in the pulse, continuous pulse-height recording of the sense signal should be an extremely powerful tool.

5. Calibration Beams

In the last section, for many of the practical problems of distortion in large detectors, we have seen the utility of calibration beams. Drift chambers being by their nature analogue devices they need fiducial marks or better infinite momentum tracks to be drawn in them.

We will review briefly the status of the two suggestions made in that field.

5.1 Pulsed X-ray Beams

One possibility is to use pulsed X-rays, as proposed by Hoffmann and Rubbia[24]. In order to penetrate a large volume of gas, the energy has to be higher than 30 keV. At this energy, electrons are extracted by means of two processes:

i) the photoelectric effect, which unfortunately gives electrons of too high energy and range,

ii) the Compton effect, which gives a continuum of energy between 0 and 10 keV (for 50 keV X-rays).

The fact that the energy spectrum is not well adapted to that of primary electrons extracted by charged particles is partially alleviated by two effects:

i) The high-energy electrons give rather flat distribution in space, while the low-energy electrons have a small range and give a peak in the observed distribution of drift distance. This "Jacobian peak" effect is clearly seen in the results obtained in the UA1 Central Detector at zero magnetic field (Fig. 10a).

ii) The magnetic field can curl up high-energy electrons and clean up the tails (Fig. 10b). A FWHM of 1.5 mm is obtained.

Calibration with X-rays has the nice advantages that diffusion is negligible and that there is no need for any special entrance windows in light detectors. In addition, there is no significant deviation at the chamber interfaces. It can therefore be used to align devices over long distances.

On the other hand, the ionization pattern produced is very different from that of a charged particle. In order not to be saturated by the predominant photoelectric effect, a low enough intensity has to be used (in UA1, 400 X-rays/beam) extracting one useful Compton electron every few cells. This Compton electron gives rise, by thermalization, to a blob of electrons which have properties that are very different from those of the electrons spread along a charged particle track. In particular, they all arrive on the sense wire at the same time, but from pulse to pulse their measured drift time will fluctuate because they are not created along a locus of equal drift time to the wire (see Fig. 6). This can be contrasted with charged particle tracks where the closest primary electron is measured.

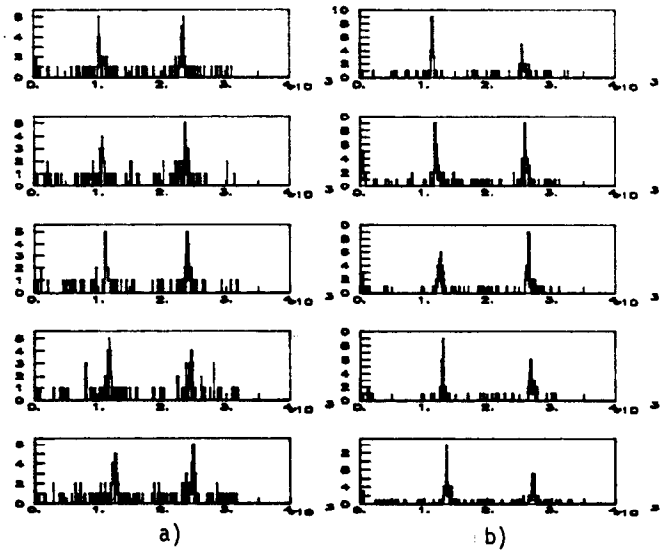

Fig. 10. UA1 X-ray beams as seen on one wire of the central detector. Bin width 8 ns. Around 2000 shots a) at zero magnetic field, b) at a field of 2.8 kG.

Therefore the X-ray beam gives intrinsically a wide distribution, which has to be averaged over many pulses. The mean drift distance measured is different from that of a real track in a way which is dependent on the shape of the loci of equal drift time to the wire and on the magnetic field.

Let us add that we have noticed a large background of X-rays scattered in the collimator and in the walls of the detector.

5.2 UV Laser Beam

A much closer simulation of a charged track can, in principle, be made with pulsed UV laser beams.

Direct photoionization of some impurity has not been attempted up to now because with known substances, it was necessary to work in the vacuum UV region. However, the "discovery" of the tetrakis(dimethylamine)ethylene (TMAE) (see, for example Ref. 11) which has an ionization potential of 5.4 eV would allow the use of relatively close UV lamps (not necessarily lasers since the needed intensity is small) at $\lambda \approx 240$ nm. This line of research has not, to my knowledge, been explored yet.

Following the work of Seiler and collaborators[26] and independently of Bourotte and Sadoulet[27] all groups involved in the field have used double photon absorption which allows one to work in the close UV region (typically 340 nm).

The basic process is shown schematically in Fig. 11a. A first photon excites the molecule usually to a virtual state. This virtual state lives for a time $\tau \simeq 10^{-16}$ s. If a second photon arrives during that time, it can ionize the virtual state. The ionization rate is, of course, quadratic with respect to the flux. When the intermediate states exist (Fig. 11b) cross-sections are much larger and one speaks of double-step processes. One can show[28] that if the latter process is at work, at low laser energy density, the pulse-height dependence is quadratic with the laser intensity. At an energy density dependent on the first-step excitation cross-section σ_1 and on the ratio between the laser pulse length and the lifetime of the intermediate state, the first transition is saturated and the dependence becomes linear.

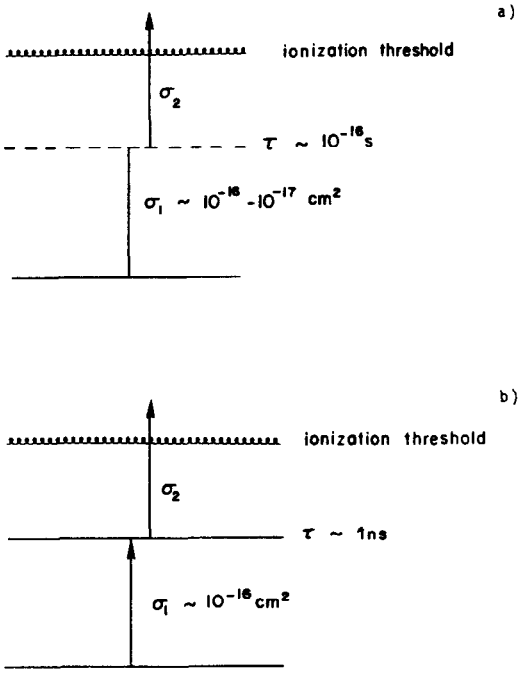

Fig. 11. Double-photon and double-step process.

This is indeed what is observed experimentally. Recently the UA1 group have been doing careful measurements[28,29] (Fig. 12) with a N_2 laser at 337 nm and a pulse length of 300 ps, and have found the expected behaviour with a transition between the quadratic and the linear region at 20 $\mu J/mm^2$.

This result was obtained without specifically adding any impurity to the Ar-C_2H_6 mixture. If interpreted in terms of the above model, it gives a cross-section $\sigma_1 \simeq 2 \times 10^{-16}$ cm^2 which is quite reasonable.

This measurement significantly clarifies the mystery of pulses, observed by various groups[27,30] without specifically adding any impurities, which showed linear dependence: the laser energy density was indeed sufficient to be in the saturation region. However, the ionizable impurity is not yet identified. This is not surprising since with reasonable values of σ_2 (10^{-18} cm^2) its concentration may be as low as 10^{-12}!

It is clear that, under these conditions, one would like to control the impurity, and for substances with the right excitation levels and the right auto-ionization levels, a very small concentration would be necessary to

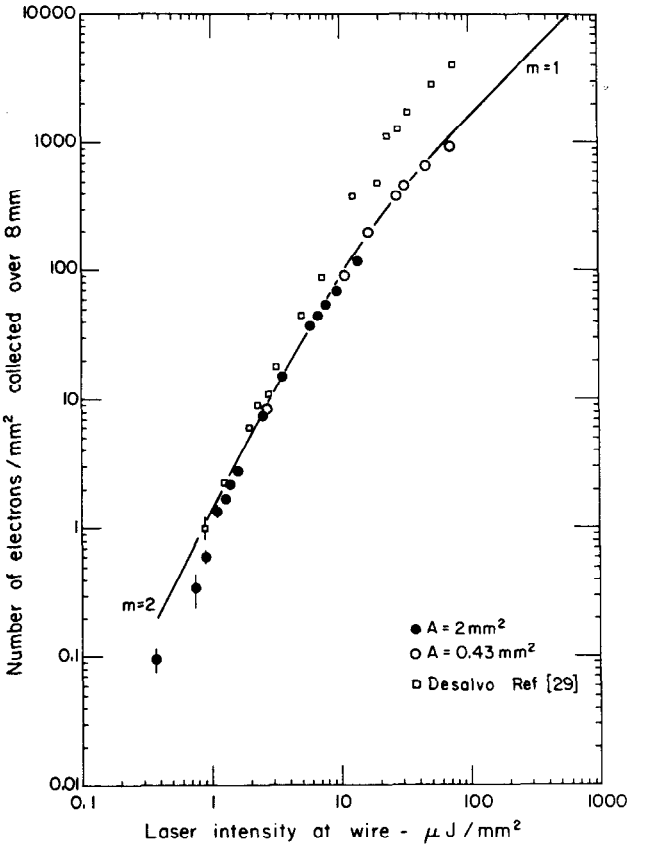

Fig. 12. Number of electrons per unit area and per 8 mm as a function of the laser energy density (Ref. 28). Squares: results of Ref. 29 obtained in a different chamber with a less accurate measurement of the area.

allow ionization by relatively small energy lasers. Up to now, no "magic" substance has yet been identified. Two compounds are known to increase ionization. Diethylaniline[27] (ionization potential = 7 eV) at a concentration of approximatley 10^{-5} and Nickelocene[26] (ionization potential = 6.5 eV). We have recently used that impurity at the level of 1.5×10^{-6} concentration and observed a factor of 7 increase in the yield (Fig. 13). This is not much, but if the absorption spectrum of Nickelocene has a broad maximum[31a] around 337 nm (3.67 eV) the photoionization spectrum[31b] has a dip around (7.3 eV) (Fig. 14). We have tried without success other substances such as anthracene, tetracene, pentacene, α naphthylamine and ferrocene at a concentration of the order of 10^{-6}.

In order to use this method practically to calibrate large drift chambers, one faces two problems: in order to produce *straight* tracks over significant distances the laser beam has to be diffractively limited (at least in one direction; such a beam of 0.6 mm thickness at 337 nm can be used over 2 m). Unfortunately, diffractively limited lasers in this wavelength are very expensive (quadrupled Neodymium Yag lasers) and even N_2 lasers with very poor beam quality are not cheap.

Hilke[30] made an important step forward by designing with Neracher of Multilasers* a double-cavity N_2 laser which is limited by diffraction in one direction.

Following in the same direction, the UA1 Collaboration made a contract with Multilasers for the design of a very small two-cavity N_2 laser ($180 \times 120 \times 32$ mm^3), which could be mounted directly on the chambers. The

* Multilasers, BP155, 1218 Grand-Saconnex, Geneva, Switzerland.

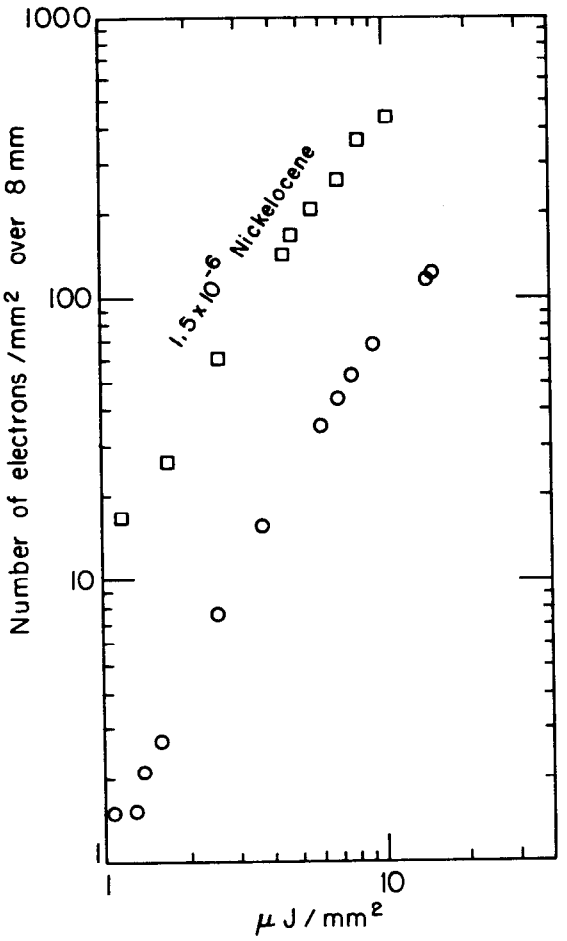

Fig. 13. Increase of signal when introducing Nickelocene at a concentration of 1.5×10^{-6}.

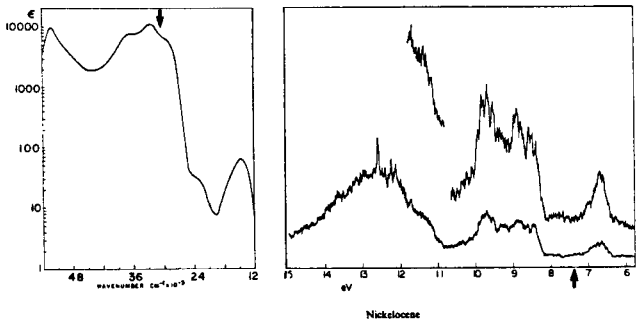

Fig. 14. a) Absorption spectrum of Nickelocene (in solution) around 337 nm. b) Photoionization spectrum of Nickelocene (from Ref. 31).

performance of the prototype is quite satisfactory. The energy in the dense spot is 30 μJ; its dimension as a function of the distance is given in Fig. 15. It is nearly diffraction limited in the narrow direction and its FWHM of 0.7 mm is maintained over 1 m (within 0.1 mm). This shows that with an afocal system of magnification 1, making the image of the laser at 1 m, a straight beam (within 0.1 mm) can be achieved over 2 m. Moreover, over the same length its effective area will be constant. This is important because, with the laser intensity we have at our disposal and our requirements to make three beams per laser, we are working in the

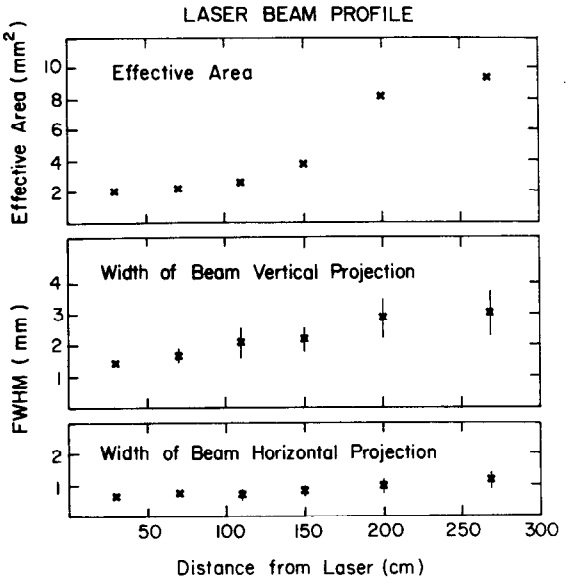

Fig. 15. Optical characteristics of the MOPA 2000 laser (designed by Multilasers) used by the UA1 Collaboration.

quadratic region where the number of electrons per cm of track is inversely proportional to the area.

The cost of the laser components is sufficiently small that we can afford to build ourselves 40 lasers providing 120 beams in the UA1 central detector.

References

1. B.D. Hyams, High Resolution in Silicon Strip Detector, Talk at this conference.
   A. Bross, High Precision CCD detector, Talk at this conference.
2. See, for example,
   V. Palladino and B. Sadoulet, Nucl. Instrum. Methods 128, 323 (1975) and Lawrence Berkeley Laboratory Report LBL-3013 (1974).
   F. Sauli, CERN 77-09 (1977).
   B. Sadoulet, Phys. Scripta 23, 433 (1980).
   J. Jaros, SLC Workshop Notes CN # 51, SLAC (Dec. 1981).
3. W.W.M. Allison and J.H. Cobb, Ann. Rev. Nucl. Part. Sci. 30, 253 (1980).
4. P. Lenard, Ann. Phys. (Germany) 12, 714 (1903).
5. W. Farr et al., Nucl. Instrum. Methods 154, 175 (1978).
6. E.J. Kobetich and R. Katz, Phys. Rev. 170, 391 (1968).
7. J.H. Parker, Jr., and J.J. Lowke, Phys. Rev. 181, 290 and 302 (1978).
8. E.B. Wagner, F.J. Davis and G.S. Hurst, J. Chem. Phys. 47, 3138 (1967).
9. H. Drumm et al., Nucl. Instrum. Methods 176, 333 (1980).
10. A.H. Walenta and C.M. Ma, quoted in Proc. ISABELLE 1981 Summer Workshop, Brookhaven National Laboratory, Upton, NY, BNL 51443 (1981).
11. E. Barrelet et al., A two-dimensional, single photoelectron drift detector for Cherenkov ring imaging, CERN-EP/82-09, 22 January 1982.
12. F. Piuz (CERN), private communication.
13. V.J. Baskakov et al., Nucl. Instrum. Methods 158, 129 (1979).
    A.J. Alikhanian et al., Nucl. Instrum. Methods 158, 137 (1979).

14. G. Charpak and F. Sauli, Phys. Lett. 78B, 523 (1978).
15. A. Barbaro Galtieri, Tracking in the PEP-4 TPC, Talk at this conference.
C.K. Hargrove, Tests of the TRIUMF TPC, Talk at this conference.
16. B.A. Dolgoshein et al., Serpukhov preprint, 1981, and B.A. Dolgoshein, private communication.
17. B.A. Dolgoshein, private communication.
18. A.H. Walenta, IEEE Trans. Nucl. Sci. NS26, 73 (1979).
19. P. Rehak and A.H. Walenta, IEEE Trans. Nucl. Sci. NS27, 54 (1980).
T. Ludlam et al., Nucl. Instrum. Methods 180, 413 (1981).
20. a) A.H. Walenta, Talk given at the 1981 ISABELLE Summer Workshop at Brookhaven National Laboratory.
b) See also the LEP letter of intent from the Lund-Siegen-Max Planck Institute-NIKHEF-ETH-Geneva-Lausanne-LAPP-Frascati-Florence-Madrid-Beijing-Hofei-Hawaii-CalTech-Oklahoma State-Carnegie Mellon-Princeton-Yale-Harvard-MIT Collaboration.
21. M. Calvetti, Talk at this conference.
22. K. Sumorok, UA1 Technical note 81-25, CERN 1981.
23. a) B. Sadoulet, Comments on charged particle detectors for the $\bar{p}p$ large solid angle detector, CERN $\bar{p}p$ Note 16 (May 1977).
b) D. Friedrich et al., Nucl. Instrum. Methods 158, 81 (1979).
c) M. Calvetti and B. Sadoulet, UA1 Technical Note 80/06 CERN, 29 January 1980.
24. H. Hoffmann and C. Rubbia, CERN $\bar{p}p$ Note 54, August 1978.
25. M. Rijssenbeek, UA1 Collaboration, private communication.
26. H. Anderhub, M.J. Devereux and P.G. Seiler, Nucl. Instrum. Methods 166, 581 (1979) and 176, 323 (1980).
27. J. Bourotte and B. Sadoulet, Nucl. Instrum. Methods 173, 463 (1980).
28. C. Cochet et al., to be published.
29. M. Desalvo and R. Desalvo, preprint CERN/SPS 81-23 (1981), submitted to Nucl. Instrum. Methods.
30. H. Hilke, Nucl. Instrum. Methods 174, 145 (1980).
31. a) D.A. Scott and R.S. Becker, J. Chem. Phys. 35, 516 (1961).
b) D.W. Turner et al., Molecular photoelectron spectroscopy (Wiley-Interscience, London, 1970).